H-Atom Electron-Spin Polarization in Irradiated Water and Ice Confined in the Nanopores of Vycor Glass†

Valery F. Tarasov, Sergey D. Chemerisov, and Alexander D. Trifunac*

Chemistry Division, Argonne National Laboratory, Argonne, Illinois 60439

Received: June 18, 2002; In Final Form: November 15, 2002

Chemically Induced Dynamic Electron-spin Polarization (CIDEP) in radiolytically generated H atoms in water-saturated Vycor glass is observed at different temperatures (+29 to −94 °C) by time-resolved pulsed EPR spectroscopy. The kinetics of polarization is investigated by means of the numerical solution of the stochastic Liouville equation (SLE) as applied to a two-site kinetic model. The experimental results are quantitatively simulated assuming that the H atom is one of the partners of the random (or triplet geminate) radical pairs and that the Heisenberg spin−spin exchange interaction is the only inter-radical interaction in such pairs. The recombination of H atoms with radical pair partners is a spin-selective reaction with activation parameters close to those of H-atom diffusion. It is shown that the rate of longitudinal spin relaxation of the partner, the rate of encounters, and the rate of the spin-selective recombination of the H atom with a partner are the most important kinetic parameters defining the observed time evolution of CIDEP. The kinetics of the CIDEP is defined mostly by the polarization generated in random pairs. The contribution of CIDEP from the geminate triplet radical pairs is important only at short times.

1. Introduction

It has been observed that the electron spins of H atoms radiolytically generated in wet and water-saturated nanoporous materials such as zeolites[1] and porous silica materials[2] are polarized. Qualitatively, the polarization conforms to the rules of chemically induced dynamic electron polarization (CIDEP).[3,4] It was found that time evolution of the CIDEP detected by time-resolved pulsed EPR (TR pEPR) spectroscopy strongly depends on the temperature, the characteristic sizes of pores, and the chemical composition of materials.[1,2] In NaY and HY zeolites two or more spectroscopically distinguishable electron-spin polarized H atoms are generated in the same material.[1,2] Thus, the observation of CIDEP can be utilized to investigate the chemical properties of confined water and ice in the cavities of wet nanoporous materials and the physical and chemical properties of the materials and interfaces.

The slow kinetics of the CIDEP rise and decay is one of the inherent features of the H-atom CIDEP in wet and water-saturated nanoporous materials.[1,2] On one hand, one would be inclined to think that the polarization is controlled by bimolecular processes much as it develops in pure water or ice[5,6] where the kinetics is also slow. On the other hand, the concentration of H atoms and paramagnetic centers is typically too small[1,2] to provide such kinetics for the H atoms confined in a particular cavity, while the diffusive migration of H atoms from one cavity to another is very slow[2] as well. Another puzzling feature is that the maximum intensities of the TR pEPR signals occur at shorter times than in pure water or ice at the same temperatures. Finally, at the same temperatures the relative intensities of emissive and absorptive EPR resonance lines are very different for different materials and from those observed in pure ice or water. For instance, in the mesoporous silica MCM-41,[2] the H-atom polarization kinetics is faster than in NaY zeolite and the emission dominates. For the NaY zeolite the intensities of the absorptive and the emissive polarization are nearly equal.

These peculiarities have been ascribed to the effects of restrictions of the H atom's (and/or paramagnetic center's) diffusion in the nanoscopic cavities filled by ice or liquid water.[1,2] None of them have been explained even qualitatively. It is unclear how the confinement disturbs the CIDEP of H atoms, what is the physical meaning of the CIDEP kinetics, and what are the main processes that contribute to the CIDEP. It is worthwhile to note that similar features were observed in the H atom's CIDEP in some solid insulators[7,8] at much higher temperatures. Thus, though the experimental observations are unique and unavailable in other spectroscopies, the phenomenon is not yet understood sufficiently to be useful for applications.

In this paper we present experimental results and theoretical analysis of CIDEP of the H atoms produced radiolytically in water-saturated Vycor glass in the temperature range from +29 °C to −94 °C. A theoretical model is developed, based on the theory of CIDEP,[3,4] modified by using a two-site approximation instead of diffusion in a restricted space.[9,10] Such an approach suffers from oversimplification but allows efficient computation of the kinetic problem. We show that the model quantitatively accounts for all the features of experimental observations.

2. Experimental Section

2.1. Sample Preparation. 7930 Vycor glass was obtained from Corning in the form of cylindrical rods of 3 mm o.d.. The glass was cleaned up by heating in 30% hydrogen peroxide solution for 2 h. After that it was washed in deionized water three times and stored in water. Just before use, the measured amount of Vycor glass was placed in a Pyrex tube and pumped out for a half-hour at room temperature. After that the

† Work performed under the auspices of the Office of Science, Division of Chemical Science, US-DOE under contract number W-31-109-ENG-38.

* To whom the correspondence should be addressed.

10.1021/jp021438j CCC: $25.00
Published on Web 01/21/2003

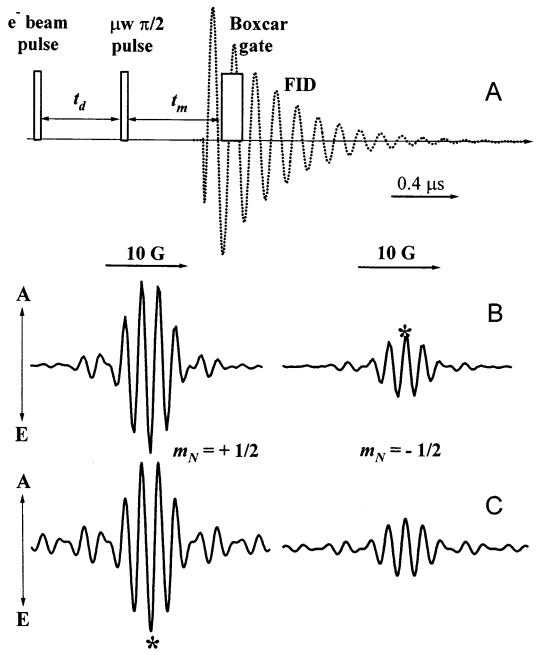

Figure 1. (A) Pulse sequence (t_d is the time delay between electron beam and μw pulses, t_m is the constant 0.3 μs delay between the μw pulse, and the acquisition of the FID) and free induction decay (FID, dotted line) of the electron-spin transverse magnetization. (B) Figure 2. Field-swept-FID-spectra of TR pEPR from polarized H atoms in water-saturated Vycor glass. Resonant magnetic fields $m_N = +1/2$ (low-field resonance) and $m_N = -1/2$ (high-field resonance) are labeled by asterisk. The width of the "spectral line" equals approximately twice the amplitude of the μw field. The shape strongly depends on the boxcar gate. When the latter approaches infinity, the signal B approaches the "true" EPR resonance signal. (C) Numerical solution of SLE as applied to a two-site kinetic model (see text). Numerical solutions slightly overestimate the contribution of the side beats due to idealization of the microwave pulse shape.

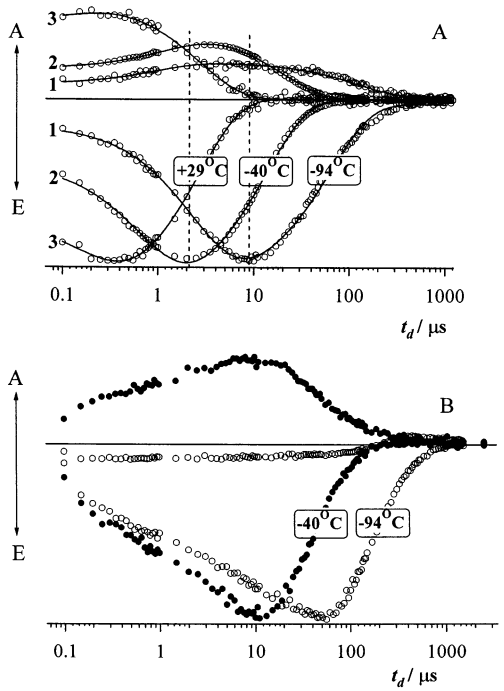

Figure 2. (A) Kinetics of the H-atom longitudinal magnetization in water-saturated Vycor glass (open circles) at −94 °C (traces 1), −40 °C (traces 2), and +29 °C (traces 3) and the fits (solid lines) by biexponential function (eq 1). The rate constants k_{dec} are nearly the same for both the absorptive and emissive lines, but at lower temperatures (< −60 °C) decay of the positive signal is slower than that of the emissive line. This suggests an additional mechanism of positive polarization, which is more effective at lower temperatures (see discussion). (B) Kinetics of the H-atom longitudinal magnetization in bulk ice at −94 °C (open circles) and −40 °C (filled circles). The rise of the signals seems to obey second-order kinetics while the decay is monoexponential with very good accuracy. It suggests that the decay of signal is controlled by longitudinal spin relaxation.

temperature of the samples was gradually increased to 450 °C during 2 h. Then the sample was baked in a vacuum ($\sim 10^{-5}$ Torr) at 450 °C for 4 h. After cooling to room temperature the sample tubes were left attached to the vacuum manifold to be further loaded.

Water was degassed by four freeze−pump−thaw cycles. Activated Vycor glass samples were then saturated with H_2O overnight at room temperature (vapor pressure of water ~20 Torr). After that the samples were evacuated again at 77 K and sealed.

2.2. Experimental Setup and Procedure. Time-resolved EPR spectra were obtained using a home-built pulsed EPR setup.[11] A sample tube was placed at the center of a Pyrex cooling jacket (10 mm o.d.). Under irradiation Pyrex does not yield spin centers that can interfere with transient H-atom signal from the Vycor sample. Temperature control was realized using nitrogen gas passed through a coil immersed in a liquid nitrogen bath, heated to the desired temperature, and passed through the Pyrex jacket.

To radiolyse a sample, typically 100 ns, 40 nC electron bean pulses from a 3 MeV Van de Graaff electron accelerator were used. The sample-average dose was 20 Gy/pulse. The temperature rise in the sample due to the electron-beam current was less than 1.5 °C. The $\pi/2$ (25 ns) μw pulses were synchronized (Figure 1) with the electron-beam pulses to program the delay time t_d between them. The dead time of the spectrometer (after the microwave pulse) was 250ns. Therefore, the $t_m = 0.3$ μs time delay preceded the acquisition of the free indduction decay (FID) signal.

To obtain field-swept-FID-spectra at a definite time delay, the FID signal was acquired by boxcar integration (typically 100 ns boxcar gate) as a function of the magnetic field B_0 of the EPR spectrometer. The field-swept-FID-spectrum (trace B in Figure 1) consists of "wiggles" due to transient nutations of the electron spin off resonance. The maximum intensity of oscillation (labeled by a star in Figure 1B) is at resonance field. To obtain the kinetics of longitudinal magnetization (Figure 2A,B) the FID signal was sampled by boxcar integration as function of delay time t_d (Figure 1A) between the electron beam and microwave $\pi/2$ pulses.

3. Experimental Results

Vycor (Figure 2A). TR pEPR spectra from the polarized H atoms (traces B in Figures 1) in water-saturated Vycor glass are doublets comprised of low-field ($m_N = +1/2$) emissively (negatively) polarized (E) and high-field ($m_N = -1/2$) absorptively (positively) polarized (A) resonance lines. (m_N is the nuclear magnetic quantum number.) The intensities of the lines are different. The emissive low-field line is always more intense than the high-field positively polarized line. Thus, the polarization is of E/A + E type. The origin of the additional net E polarization has been surmised[1,2] to arise from the flip-flop electron−nuclear spin transitions within the point of the electron−nuclear spin levels crossing (so-called radical pair mechanism ST_RPM[3,4]). The multiplet E/A polarization (or the appearance of positive polarization of the high-field resonance line) was assumed to be due to ST_0RPM.[3,4]

As illustrated in Figure 2A, a decrease in temperature shifts the positions of maxima of both absorptive and emissive polarizations into longer times. There is a clear correlation between the maximum intensities and their position on the time axis. The lower the temperature the stronger the relative emissive polarization, and the later the time of the observation of maximum polarization. This correlation suggests the existence of a common kinetic process for the creation of both negative and positive polarization. However, the time of maximum positive polarization for the medium temperatures (trace −40 °C in Figure 2A) does not coincide perfectly with that of the negative polarization. Moreover, in the case of low temperatures (trace −94 °C in Figure 2A), the kinetic curve of the positive polarization shows two poorly resolved maxima. Therefore, it is unlikely that only ST_0RPM contributes to the positively polarized signal.

The absolute intensities of TR pEPR signals also depend on temperature. The intensity of negative signal at −94 °C is much lower than that at −40 °C, but the intensity of the negative polarization at higher temperature is lower than that at − 40 °C. Decrease in temperature causes an increase in viscosity; in turn it increases the efficiency of ST_RPM polarization. That explains qualitatively the initial increase in the intensity of polarized signal when temperature decreases from +26 °C to −40 °C. At the same time, the increase of viscosity decreases the rate of the encounters. The increase in the efficiency of flip-flop transitions can be canceled by this decrease. In other words, it is not obligatory that the intensity of the negative polarization must increase continuously when the temperature decreases.

The kinetic curves of the EPR signals (Figures 2A) can be simulated (solid lines in Figure 2A) in terms of the biexponential function given by eq 1

$$I(t) = A_0 + A_{grw}\exp(-k_{grw}t) + A_{dec}\exp(-k_{dec}t) \quad (1)$$

The rate constants k_{grw} and k_{dec} differ noticeably from each other for a given sample but are nearly the same for both the low-field emissive and the high-field absorptive lines. Unfortunately, the experimental accuracy and the fact that the kinetics are not exactly biexponential in nature do not allow for an accurate determination of the activation parameters of the k_{grw} rate for both positive and negative polarizations. The uncertainty in experimental data is mostly due to changes of sample characteristics caused by the intense and prolonged electron irradiation. Analysis of the decay of the emissive signal (Figure 3) can be done more accurately. It follows from Figure 3 that the activation energy of the negative polarization decay is between 10 and 14 kJ mol^{-1}. Using these data one can conclude that activation energy for the processes involved in the decay of polarization (chemical decay of H atoms, spin relaxation) exhibit similar activation energy as observed for the H-atom diffusion in pure ice (E_{diff} = 12.6 kJ mol^{-1}).[5]

Bulk Ice (Figure 2B). CIDEP of H atoms generated in ice by electron pulse radiolysis has been previously investigated.[5] We reproduced some experimental results to clarify the differences in CIDEP kinetics of H atoms produced by the radiolysis of bulk hexagonal ice and ice confined in pores of Vycor glass. For the bulk water/ice, CIDEP intensities have square dependence on the radiation dose,[5,6] while for the Vycor glass they have linear dependence. The rising part of kinetics in bulk ice is most likely due to random H···H bimolecular encounters.[5] There seem to be no such encounters in the confined ice. The decay of CIDEP in bulk ice is controlled[5] by the electron-spin relaxation (almost certainly due to spin exchange with the OH radicals) and appears monoexponential with high accuracy. For the confined ice the decay of the CIDEP signal is only approximately monoexponential and whether it is due to spin lattice relaxation or not is questionable.

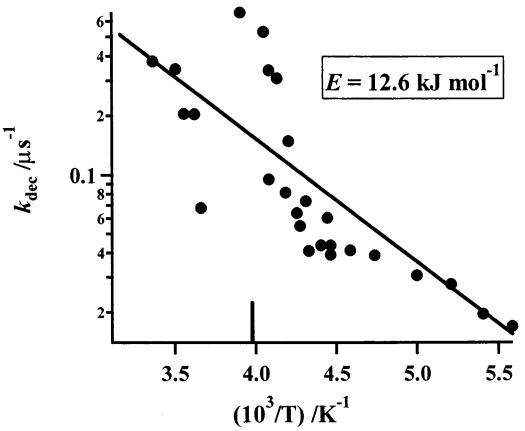

Figure 3. k_{dec} (filled circles) for the emissive low-field resonance line of H atoms in water-saturated Vycor glass (Figure 2) as a function of temperature. Vertical stick indicates the expected temperature of the melting point of confined ice in Vycor cavities (~ 20 °C). Solid line is not the best fit of the experimental results but the plot of function $10^{-6}k_{dec} = 56 \times \exp(-12.6/RAT)$, where 12.6 kJ mol^{-1} is the activation energy of the H-atom diffusion in hexagonal ice.[5]

The interesting feature of the bulk-ice radiolysis is that the high-field line in the EPR spectra from H atoms is emissive at low temperatures (trace −94 °C in Figure 2B). Whether this is due to the contribution of singlet geminate radical pairs,[5] or due to electron exchange between stronger negatively and weaker positively polarized H atoms, or due to some unknown process is unclear at present.

What is important for this work is that the kinetic traces obtained at the same temperatures and doses of irradiation are very different (compare Figures 2A and 2B) for the confined and bulk ice, respectively. One can suggest three possibilities. First, the restricted diffusion of H atoms within the confined clusters of water/ice is responsible for these differences. Second, H atoms diffuse along the surface of the Vycor cavity's walls and suffer additional mechanisms of spin relaxation. Third, the mechanism of the CIDEP in confined water/ice is different from that in bulk water/ice due to different structure of the latter. In this paper we focus on the first possibility.

4. The Model

It was shown before[2] that the main source of H atoms in heterogeneous systems is the reaction of electrons with free and surface-bound protons. If we rule out the ideas about the existence of exotic transient states[7] which can lead to the electron-spin polarization of H atoms, and if we limit ourselves to the theoretical concepts of CIDEP,[3,4] then we must assume the existence of radical pairs, where the H atom is one of the partners. Radiolysis of the confined water/ice in the nanopores of Vycor glass and Vycor glass itself creates several possible candidates for the other partner. These are OH radicals, defects:[12,13] (≡SiO, ≡Si, ≡Si−Si≡), and Boron centers. In porous materials, the accessibility of these defects is an issue, due to the fact that H atoms preferably stay inside the pore in the time frame of our experiment and interact with the defects on or near the surface. The species listed above are generated in processes that occur independently of the generation of H atoms. At the same time there are processes that may result in geminate pairs. For example the direct dissociation of water molecules:[14] H_2O^*

→ H + OH. The reaction of triplet excitons, such as ^{3}exciton + SiOH → SiO + H, is another possible source of the geminate pairs.

In our discussion we assume that the radical pair partner to the H atom has negligible hyperfine interaction and that its *g*-factor g_b is isotropic. We assume that the isotropic Heisenberg spin−spin exchange interaction is the only spin−spin magnetic interaction between the H atom and its partner. The dipolar spin−spin interaction can be treated[8] as a correction of the intensity of Heisenberg spin−spin exchange.

In the rotating frame (ω_0) the model spin Hamiltonian H_{RP} of the radical pair (RP) $a\cdots b$ (where indexes *a* and *b* stand for H atom and partner, respectively) is

$$H_{RP} = H_a + H_b + H_{ex} + H_{\mu w} \tag{2}$$

$$H_a = (\omega_a - \omega_0)\cdot S_{az} + A\mathbf{S}_a\cdot\mathbf{I} - \omega_0 I_z \tag{2a}$$

$$H_b = (\omega_b - \omega_0)\cdot S_{bz} \tag{2b}$$

$$H_{\mu w} = \omega_{1a} S_{ax} + \omega_{1b} S_{bx} \tag{2c}$$

$$H_{ex} = -J(r)\cdot\left(\frac{1}{2} + 2\mathbf{S}_a\cdot\mathbf{S}_b\right) \tag{3}$$

Here $\omega_i = g_i\beta B_0$ ($i = a$ and *b*), g_i are the *g*-factors of radicals, β is the Bohr magneton, B_0 is the magnetic field of EPR spectrometer, ω_0 is the frequency of the EPR spectrometer, $\omega_{1i} = g_i\beta B_1$, B_1 is the strength of the microwave field, and *A* is the hyperfine interaction (HFI) in the H atom.

The most commonly used convention[3] employs an exponential dependence of the exchange interaction $J(r)$ between two particles at a distance *r* between them:

$$J(r) = J_0 \exp\left[-\frac{(r-R)}{\lambda}\right] \tag{4}$$

J_0 is the intensity of Heisenberg exchange interaction at the distance $r = R$ of the closest approach of radicals, and λ^{-1} is the steepness of the exchange potential. Rather than use the function eq 4 we assume that $J(r)$ is proportional to the step-function eq 5:

$$J(r) = \begin{cases} J_c \text{ if } r \le R + \lambda \\ 0 \text{ if } r > R + \lambda \end{cases} \tag{5}$$

As a convincing test of reasonability of this approximation we calculated the EPR spectra (Figure 4, traces 1 and 2) of a hypothetical radical pair enclosed in the 13 Å spherical cavity. Spectrum 2 was calculated for the exponential exchange interaction eq 4 using the time-window method[10] and accurate numerical solution of the SLE for diffusing radicals. Spectrum 1 was calculated for the exchange taken as a step-function (eq 5) in terms of the theoretical model considered in this paper. The close agreement between these two spectra is obvious.

As mentioned above, we assume that H atoms diffuse within the water or ice clusters. It is known[15] that the Vycor glass cavities are cylinders. In our case the diameter of the cylinders is about 40 Å,[16] which is too large to assume one-dimensional diffusion. Therefore, a strict theoretical model must consider the diffusion in a cylinder of a finite length. In doing so, definite suggestions about the physical-chemical properties of the media inside of a cavity must be formulated. H-atom diffusion in ice is not isotropic,[5] and this can be very important for the nanoscale diffusion. It is also known that the water is liquid[17] in the immediate vicinity of the walls even at cryogenic temperatures,

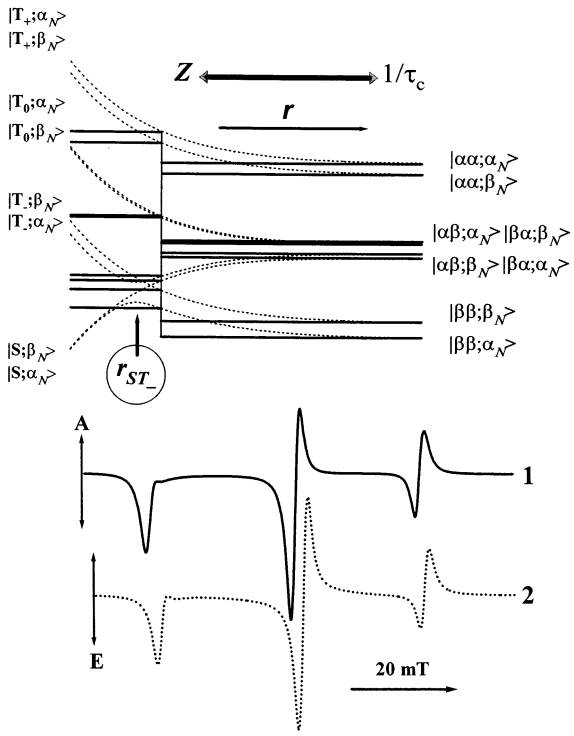

Figure 4. Top. Correlation diagram of the electron−nuclear spin states for a radical pair in the exchange potential given by eq 4 (dashed lines) and eq 5 (solid lines). Bottom. cw TR EPR spectrum calculated using numerical solution of the SLE as applied to a two-site kinetic model (trace 1) with the spin−spin exchange interaction given by eq 5. Trace 2 is the cw TR EPR spectrum calculated[24] using numerical solution of the SLE as applied to diffusional motion of radicals in the exchange potential given by eq 4. Radicals are in a spherical cavity. $J_0 = J_c = -1.5 \times 10^{10}$ rad/s and $k_s = 0$ were used in both cases. All other parameters were recalculated using formulas given ref 10. The differences in the spectral shapes are due to the fact that use of a time window (trace 2) results in overestimation of the contribution from short-lived radical pairs.

so the medium is not homogeneous. Nothing is known about the effects of dispersion interactions of H atoms with the walls of a cavity or the diffusion of H atoms. At the same time, nothing is known about the motion of a partner radical. Most probably the partner is fixed in the walls of a cavity or even inside of the wall. Fortunately, we do not need a detailed description of the H-atom diffusion inside of the cavities. As long as the distance between the H-atom and its partner is so large that the inter-radical magnetic interactions can be neglected, the detailed picture of motion is of no importance. Therefore, it is quite reasonable to utilize, as a first approximation, the effective frequency of encounters *Z* between the H atom and its partner. *Z* is assumed to be independent of time and coordinates. By doing so we introduce some effective parameters, but these parameters can be tested when the details about the diffusion of H atoms become available from future studies.

From the kinetic point of view, the correctness of this approximation is warranted by the fact that the diffusing particle enclosed in a cavity of arbitrary shape with inert walls evolves in time to a state where the probability to find a particle at any arbitrary point inside of a cavity does not depend on the coordinates of the particle. We call this "filling out the cavity". Of course, the duration of filling out of a cavity depends on the geometry of a cavity, the viscous properties of the medium inside of the cavity (water or ice), and on the interaction of the diffusing particle with the walls of the cavity. For instance, the time of filling out of a spherical cavity with the reflective wall

is $(3V/4\pi)^{1/3}(r_A/\pi D_A)$,[10] where V is the volume of the cavity, r_A is the radius of the particle ($r_A \ll V^{1/3}$), and D_A is its diffusion coefficient. Using this formula as a crude estimate for the cylinder of 1 μm length and 40 Å diameter, we calculate that H atom will take about 0.2 μs to fill such a cavity at room temperature if the adsorption of H atoms by the walls can be neglected. The time of filling out places a limit on the correctness of our kinetic approach only in the case of initially inhomogeneous distribution of H atoms. If this distribution is homogeneous from the beginning, the problem of correctness is reduced to the similar problems existing for the kinetic description of bimolecular reactions.[18]

The definition of $J(r)$ (eq 5) means that the radical pair comprised of the H-atom and its partner is found in two states called "contact" and "separate". Z^{-1} and τ_c are the lifetimes of the separate and contact states, respectively. Correspondingly, the density matrix of a radical pair is comprised of the density matrices (vectors in Liouville space) of the radical pairs in the contact ($\rho_c(t)$) and in the separate ($\rho_s(t)$) states. Then the stochastic Liouville equation for the state vector ($\rho_c(t)$ / $\rho_s(t)$ / $\rho_e(t)$) of the system in the Liouville spin space can be written as follows:

$$\begin{pmatrix}\dot\rho_c(t)\\ \dot\rho_s(t)\\ \dot\rho_e(t)\end{pmatrix} = \begin{pmatrix}L_c - \tau_c^{-1} - k_e & Z & 0\\ \tau_c^{-1} & L_s - Z - k_e & 0\\ k_e & k_e & L_s\end{pmatrix} \cdot \begin{pmatrix}\rho_c(t)\\ \rho_s(t)\\ \rho_e(t)\end{pmatrix} \quad (6)$$

where $\rho_e(t)$ is the state vector for the system in which one of the radicals lost its partner in the monoexponential process k_e ($k_e = k_a + k_b$, k_a and k_b are the decays of H atom and partner due to side reactions). L_c and L_s are the Liouvillian superoperators of the contact and separate radical pairs, respectively:

$$L_c = -iH^{\times}(J{=}J_0) - \frac{1}{2}k_s P_s^{\times} + W \quad (7a)$$

$$L_s = L_c(J{=}0;k_s{=}0) \quad (7b)$$

$H^{\times} = [H,...]_-$ and $P_s^{\times} = [P_s,...]_+$ are the superoperators, commutator and anticommutator, respectively, P_s is the projector operator on the electron-spin singlet manifold.

The Liouvillian contains the spin-selective (operating only in the contact state) decay of the radical pair. This is described by the projector P_s onto the singlet-electron-spin manifold and the rate constant of recombination k_s within this manifold.

To complete the discussion of the separate and contact states the ST_RPM should be mentioned. This mechanism is frequently used to give a qualitative interpretation of the net negative spin polarization. It is based[19,20] on the theory of nonadiabatic magnetic transitions between the electron−nuclear spin states of a radical pair in the distinct region of distances $r_{ST\_} \approx R + \lambda \ln(2|J_0|/g\beta B_0)$ between radicals. At first glance, the two-site model overlooks this mechanism since the model does not imply the existence of a distinctive distance $r_{ST\_}$. At the same time, the accurate numerical simulation of experimental results showed[10] that the intensity of exchange interaction between radicals of σ- and π-type is around $(1.2-2.5) \times 10^{10}$ rad/s at the distance R of the closest approach of radicals instead of the required 3×10^{10} rad/s (and more) for X-band EPR spectrometers. It appears that the CIDEP due to the nonadiabatic transitions at the inter-pair distance $r_{ST\_}$ contributes little, if at all, to the CIDEP created at the larger distances in slowly diffusing radicals, at magnetic fields of an X-band spectrometer.

The superoperator W in eq 7 represents the spin relaxation of radicals due to stochastic interactions of spins with the bath. It is worthwhile to note that the modulation of exchange interaction and spin-selective reaction also cause spin relaxation in the system. The relaxed (equilibrium) state of the system only due to the Heisenberg spin exchange operating between the two radicals of the pair is different from the equilibrium resulting from the relaxation due to interaction of electron and nuclear spins with the bath. To avoid confusion, we call the spin relaxation due to stochastically modulated exchange interaction and the spin-selective decay "internal relaxation". The relaxation caused by magnetic interactions of radicals with the surrounding will be called "spin relaxation".

To include the spin relaxation in the model we use a Bloch presentation and neglect the Boltzman polarization. The latter seems reasonable since the signal from the Boltzman-polarized H atoms is comparatively small and the inversion of the negatively polarized signal into the positive one was not observed experimentally in Vycor glass. In Liouville space of single spin 1/2, the spin relaxation is described[9] by a Bloch superoperator

$$W_i = \begin{pmatrix}w_{1i} & 0 & 0 & -w_{1i}\\ 0 & w_{2i} & 0 & 0\\ 0 & 0 & w_{2i} & 0\\ -w_{1i} & 0 & 0 & w_{1i}\end{pmatrix} \quad (8)$$

where w_{1i} and w_{2i} ($i = a$ and b) are the rates of longitudinal and transverse spin relaxation, respectively. To build the superoperator for the three-spin system, one has to keep in mind that the tensor product of the state vectors (density matrix) is not isomorphic with the tensor product of superoperators in Liouville space (see, however, ref 9).

Pairs can be created in a specific electron-spin state (singlet or triplet, or in the coherent mixture of these states) or can be initially noncorrelated. Pairs created from radicals of different origin are noncorrelated. The initial density matrix for such a pair is the unit matrix. RPs of radicals having a common precursor can be created in a correlated spin state. It is not necessary that these pairs are contact pairs, but it is highly probable. Therefore, we assume that some fraction p_c of RPs at $t = 0$ are in contact and in a correlated state. Consequently the initial state vector of radical pairs in Liouville space is comprised of density matrices:

$$\rho_c(t{=}0) = \frac{1}{6}p_c \cdot \{\xi_T(E_4 - P_s) \cdot + \xi_S \cdot P_s\} E_2 \quad (9a)$$

$$\rho_c(t{=}0) = \frac{1}{8}(1 - p_c) \cdot E_4 \oplus E_2 \quad (9b)$$

where $\xi_T + \xi_S = 1$; E_2 and E_4 are unit operators of dimensions 2 and 4, respectively; and P_s is the projector operator on the singlet manifold in the electron-spin space. In other words the RPs are assumed to be created as spin correlated pairs in the contact state and as random pairs in the separate sate. The dissociation of OH bound to silica due to interaction with triplet excitons or electrons exemplifies the former, the RPs of H atom and independently created paramagnetic centers (Boron centers for instance) exemplifies the latter.

The calculation proceeds as follows. Initially the system develops in the resonant high or low magnetic fields B_0 during the time interval t_d after the electron pulse: $\rho(t_d) = \exp[t_d U(Z,\tau_c;B_0,\omega_1 = 0)] \cdot \rho(0)$, where $\rho(0)$ is given by eqs 9a and 9b, and U is the evolution superoperator given by eq 6. Then

the μw field ω_{1x} is switched on during the time interval t_p: $\rho(t_d + t_p) = \exp[t_p \cdot U(Z,\tau_c;B_0,\omega_1)] \cdot \rho(t_d)$. Then the system develops in the resonant magnetic field again during the time interval t_m: $\rho(t_d + t_p + t_m) = \exp[t_m U(Z,\tau_c;B_0,\omega_1)] \cdot \rho(t_d)$. The observable $|S_y\rangle(t) = \sum_{i,j}|S_{iy}\rangle_j(t)$, $i = a$ and b; $j =$ c, s, and e is plotted against $t = t_d$. It is accepted throughout the paper that $\omega_1 = 5.3 \times 10^8$ rad/s, and $t_m = 0.3$ μs. This sequence reproduces the experimental measurements except for the nonzero offset used in the experiment for practical reasons. Padé approximation with the scaling algorithm[21] which is being used in our calculations, was found to be particularly fast and accurate.

5. Discussion of Simulation Results

The goal of our modeling is to formulate and test a theoretical description of the experimental data which would be balanced between generality and simplicity (to run a numerical calculation within a reasonable computational time) and at the same time would give further insight into the physical processes in real systems. Equation 1 is a good example where simulation can be successful but is useless, until the meaning of various parameters is known.

5.1. Parameters. The magnitude of the HFI and *g*-factor for H atoms located in water or ice inside of Vycor cavities were determined from experiment: $A = 8.849 \times 10^{10}$ rad/s, $g_a = 2.0016$; the *g*-factor of partner (g_b) was proposed to be equal to 2.0023. Due to the large magnitude of A it is reasonable to suggest that $|g_a - g_b|\beta B \ll A$. Therefore, the value of g_b plays no role in the time dependence of H-atom CIDEP. Neither g_a nor A exhibited noticeable dependence on the temperature.

Each experiment taken separately can be simulated by several sets of parameters. However, the situation changes dramatically if we accept definite restrictions. We consider J_c, the exchange interaction in the contact state, as the parameter which does not depend on the temperature. The lifetime of the contact state can be estimated in two ways as $\tau_c = \lambda R/D$ (taking into account all the diffusive trajectories of the geminate encounter) and as $\tau_c = \lambda^2/D$ (taking into account only those diffusive trajectories which are enclosed within the exchange layer). In both estimates τ_c is inversely proportional to the coefficient D of mutual diffusion. Since the rate of encounters Z is proportional to D (for instance for a spherical cavity $Z = 4\pi RD/V$, where V is the available volume of the sphere[9,10]) we accept the restriction that the product of Z and τ_c should not depend on the temperature. The third restriction is that the rates of the longitudinal spin relaxation w_{1i} can only increase with the temperature. Though the restrictions accepted above effectively set limits on values of the parameters, uncertainties still remain. The main difficulty is caused by the strong dependence of kinetic curves on the spin relaxation rates in the system. The simulations given in this paper are based on the longitudinal relaxation times of H atoms measured in bulk water.[5]

Figures 5A,B, and 6A show representative experimental and calculated kinetic curves. Experimental data were obtained at +29 °C (Figure 5A, we call this high temperature), at −36 °C (Figure 5B, medium temperature), and at −94 °C (Figure 6A, low temperature). All the theoretical curves were calculated with $J_c = -2.1 \times 10^{10}$ rad/s and $Z\tau_c = V_J/V = 8.3 \times 10^{-4}$, where $V_{J=4}\pi\lambda R^2$ is the volume of exchange layer. It follows from this value that most (99.9%) of the time the H atoms are "free", i.e., they are in the separated state. Therefore, the contribution of contact RPs to the spectra is negligible, even though the spectral exchange between the contact and separate states is slow at low temperatures. It is worthwhile noting that the intensity of exchange found in these calculations is very similar to $-(1.8 - 2.5) \times 10^{10}$ rad/s found for the other radical pairs comprised of σ- and π-radicals.[10,22] Thus, the level crossing point $r_{ST\_}$ does not seem to play an important role for the pairs of the H-atom and its partner in our particular system.

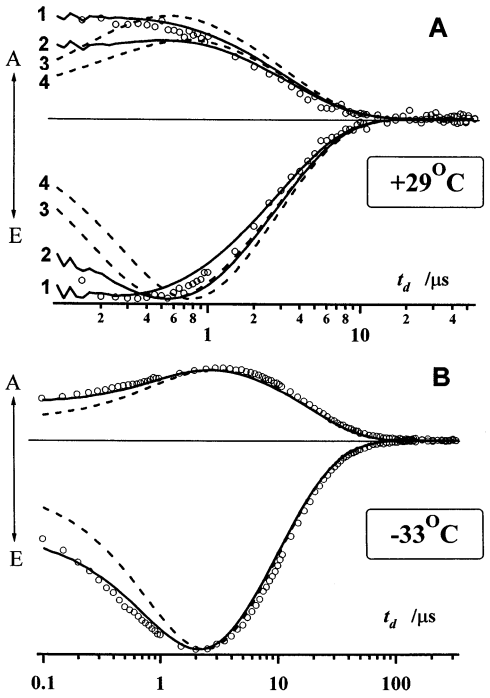

Figure 5. Kinetics of the emissive and absorptive polarization of H atoms observed under the radiolysis of water-saturated Vycor glass at +29 °C (open circles). The simulated kinetics calculated using the two-site kinetic model with the assumption of random ($p_c = 0$) and partially ($p_c = 0.16$) triplet ($\xi_T = 1$) correlated pairs are shown by the dashed and solid lines, respectively. The overall longitudinal spin relaxation rates are $8 \times 10^6 s^{-1}$ (traces 1 and 3) and 4×10^6 s^{-1} MHz (traces 2 and 4). Parameters used in these calculations are given in Table 1. (B) Same as A except temperature. $p_c = 0$ (dashed line), $p_c = 0.03$, $\xi_T = 1$ (solid line). Values of parameters used for the calculation are given in the Table 1.

The values of parameters are shown in Table 1. From these data it follows that the rate of encounters Z varies with temperature from 4×10^7 s^{-1} at +29 °C to 6.4×10^5 s^{-1} at −94 °C, which means that Z is lowered by a factor of 62. Activation energy for the diffusion of H atoms in ice is known[5] to be 12.6 kJ mol^{-1}. That implies approximately 19-fold reduction in diffusion coefficient of H atoms in ice when temperature decreases from 0 °C to −94 °C. In the experiment, the high temperature was +29 °C. Consequently, there is an additional approximately 2-fold increase in D with melting of ice and ca. 1.5-fold increase when temperature increases to +29 °C. In aggregate, the estimate predicts 56-fold increase in the diffusion coefficient. Therefore, the change in Z from 4×10^7 s^{-1} to 6.4×10^5 s^{-1} is quite reasonable and is in good agreement with the expected variation.

The actual values of Z also seem to be quite reasonable. Using the formula $Z = 4\pi RD/V$ (which is correct for the "filled out" cavity with the reflective walls) and a known value of the radius of Vycor channels of about 20 Å[16] we conclude that the length of a cylinder should be about 1.5×10^{-6} cm ($R \sim 6$ Å; $D \sim 1 \times 10^{-5}$ cm^2/s). At first glance this value appears too small. However, the H atoms need about 2 μs to travel this distance. This time is nearly the time when the polarization is still intense. Therefore, this estimate strongly supports our result.

As already mentioned, it was found that $Z\tau_c = 8.3 \times 10^{-4}$. In the case of high temperature, $\tau_c = 2 \times 10^{-11}$ s. Using the

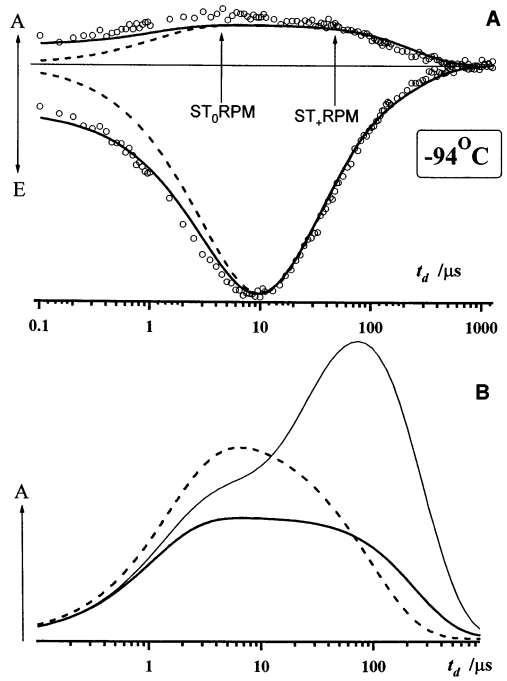

Figure 6. (A) Same as 5A and 5B except for temperature. $p_c = 0$ (dashed line), $p_c = 0.008$, $\xi_T = 1$ (solid line). Values of other parameters used for the calculation are given in Table 1. (B) ST_0RPM vs ST_+-RPM. Calculated kinetics of positive polarization for low temperature: (i) fitted to the experimental results (solid thick line), (ii) the same except that the rate of longitudinal relaxation in the radical pair is decreased by a factor of 4 (thin solid line), (iii) the positive ST_0-RPM polarization calculated in the high-field approximation with the same parameters except that the longitudinal relaxation is neglected (dashed line). Values of parameters used for the calculation are given in Table 1 for the low temperature.

TABLE 1: Values of Parameters Used in the Simulation[a]

temperature	Z/ $10^6\,s^{-1}$	τ_c^{-1}/ $10^9 s^{-1}$	k_s/ $10^9 s^{-1}$	$(w_{1a}+w_{1b})$/ $10^6\,s^{-1}$	p_c
high (+29°C)	40	48	1.6	8 (4)	0.16
medium(−33°C)	1.9	2.3	0.3	2	0.06
low (−94°C)	0.64	0.75	0.025	0.25	0.008

[a] $J_c = -2.1 \times 10^{10}$ rad/s, $A = 8.849 \times 10^{10}$ rad/s; $g_a = 2.0016$, $g_b = 2.0023$. The temperature variation of the H spin relaxation ($w_{1a} = 1.28 \times 10^5\ s^{-1}$) was neglected because the data depend on the sum of the relaxation rates of the H atom and its partner.

estimate $\tau_c = \lambda R/D$ and assuming $\lambda = 0.5$ Å, one finds that $\tau_c = 3 \times 10^{-11}$s. This coincidence is rather convincing.

It follows from the data in Table 1 that the rate constant of recombination of the H-atom and its partner in the contact and in the singlet electron-spin state k_s changes from $1.6 \times 10^6\ s^{-1}$ at high temperature to $2.5 \times 10^7\ s^{-1}$ at low temperature. Thus, the product $k_s\tau_c$ is equal to 0.03 in both temperature extremes and only weakly depends on the temperature. It turns out that the activation energy for the H-atom diffusion and recombination is about the same. If this is correct, it appears that there may be far-ranging new applications for the CIDEP of H atoms in wet microporous materials. Surprisingly, the kinetic curves can be simulated with the rate of recombination of singlet pairs far less than the diffusion control ($k_s\tau_c = 0.03 \ll 1$) limit.

Time dependence of CIDEP in the system does not depend on the rates of transverse spin relaxation w_{2i}; that was to be expected since the ratio $A/4Z = 8.8$ at high temperature and increases further when temperature decreases. As a result the coherent effects in electron-spin motion of two radicals cannot disturb either the relative intensity or shape of the spectral lines. At the same time the choice of the combined rate $w_{1a} + w_{1b}$ of the longitudinal spin relaxation strongly influences the relation between the intensities of the negative and positive polarizations and the position of their extrema (See data in Table 1 and Figures 5A,B and 6A). At low and high temperature the combined rate of longitudinal spin relaxation was found to be about $2.5 \times 10^5\ s^{-1}$ and $(4-8) \times 10^6\ s^{-1}$, respectively. T_1 of electron spin in H atom is about 23 μs ($w_{1a} = 0.025\ \mu s^{-1}$) at the temperature of ice melting.[5] Therefore, we assign the (30−15)-fold reduction of the rate of longitudinal relaxation in pairs to that of the partner. All the simulations were run at negligible rates $w_{2N} = 2w_{1N} = 0.02\ s^{-1}$ of the nuclear spin relaxation and zero rate constant k_e of th spin-nonselective decay of pairs.

The dashed lines in Figures 5A,B and 6A are calculated with the assumption that all the pairs are random. This approach gives excellent results for the decay kinetics but fails to represent the rise of CIDEP. The solid lines which cover the whole time interval of CIDEP kinetics are calculated with the assumption that a fraction (p_c, see eq 9) of radical pairs are created as contact radical pairs in the triplet electronic spin state. It was found that $p_c = 0.16$ at high temperature, 0.03 at medium temperature, and 0.008 at low temperature. This dependence of p_c on the temperature can be due to fact that the parameters of the geminate pairs are different from those we have used for the random pairs. At the same time, it is reasonable to suggest that the triplet excitons located in the walls of cavities are in deep traps and that the increase in temperature releases them from such traps.

5.2. Discussion. Initially we briefly discuss the spin dynamics in the RPs. Figure 4 (top, dashed lines) shows the correlation diagram of the spin states of an RP with the exchange potential given by eq 4. The same correlation is correct for the potential (eq 5). There are eight electron−nuclear spin states of a pair: $|m_a,m_b;m_N\rangle$ ($m = \alpha,\beta$). The state separated by a semicolon is the spin state of the H nucleus, the first position in the brackets is reserved for the electron spin of the H atom; the second position is for the electron spin of the partner. The $|\alpha\alpha;\alpha\rangle$ and $|\beta\beta;\beta\rangle$ spin states of the separate pairs ($|J(r)| \ll A$) correlate with the $|T_+;\alpha\rangle$ and $|T_-;\beta\rangle$ spin states of the $|J(r)| > A$. These states are the eigenstates of the Hamiltonian (eq 2) ($\omega_1 = 0$). They are not involved in the spin evolution due to magnetic interactions in the RP. Spin-selective recombination of the RP is forbidden for these states. For brevity we call them "inactive" states. The other six states of the separate pairs are the coherent mixtures of the $|\alpha\alpha;\beta\rangle$, $|\alpha\beta;\alpha\rangle$, and $|\beta\alpha;\alpha\rangle$ states ($F_z = m_a + m_b + m_N = +1/2$) and $|\beta\beta;\alpha\rangle$, $|\alpha\beta;\beta\rangle$, and $|\beta\alpha;\beta\rangle$ ($F_z = -1/2$). Since $(A/2B_0)^2 \approx 0.0064$, the coefficients of mixing are small. Therefore for the qualitative discussion the $|\alpha\beta,m_N\rangle$ and $|\beta\alpha,m_N\rangle$ states can be considered as the eigenstates of separate pairs ($\omega_1 = 0$).

Since the product $AJ_c < 0$, the spin state $|\alpha\beta;\alpha\rangle$ ($|\beta\alpha;\beta\rangle$) correlates with the $|T_0;\alpha\rangle$ ($|T_0;\beta\rangle$) state, while the spin state $|\alpha\beta;\beta\rangle$ ($|\beta\alpha;\alpha\rangle$) correlates with the $|S;\beta\rangle$ ($|S;\alpha\rangle$) state. Due to the strong HFI ($A = 8.849 \times 10^{10}$ rad/s), these four states are involved in efficient ST_0 mixing. Moreover, since $A/4Z > 8$ in all experimental conditions (see Table 1), the spin-selective recombination can effectively deplete these states.

The $|\alpha\alpha;\beta\rangle$ and $|\beta\beta;\alpha\rangle$ spin states correlate respectively with the $|T_+;\beta\rangle$ and $|T_-;\alpha\rangle$ spin states. For the secular Hamiltonian, these states are "inactive" in the spin-selective recombination and are not involved in the spin evolution. The nonsecular part of the HFI mixes these "inactive" $|\alpha\alpha;\beta\rangle$ ($|\beta\beta;\alpha\rangle$) states with the "active" $|\beta\alpha;\alpha\rangle$ ($|\alpha\beta;\beta\rangle$) ones resulting in sharing of the reaction character of the active states. This process is symmetric

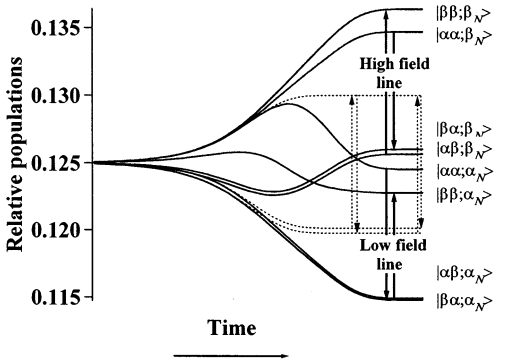

Figure 7. Kinetics of relative populations $\rho_{ii}^{rel}(t) = \rho_{ii}(t)/\sum_{j=1}^{8}\rho_{jj}(t)$ where $\rho_{ii}(t)$ is the absolute population of the ith spin state ($i = 1-8$) are illustrated. Parameters used in the calculation are given in the text. In early time the relative populations of the "active" $|\alpha\beta;m_N\rangle$ and $|\beta\alpha;m_N\rangle$ states, which are different due to ST_0RPM, decrease, since their population by spin relaxation is inefficient when the difference in populations between "active" and "inactive" states is small. At longer time the relative depletion of only $|\alpha\beta;\alpha\rangle$ and $|\beta\alpha;\alpha\rangle$ spin states ($F_z = +1/2$) develops further while the relative populations of the $|\alpha\beta;\beta\rangle$ and $|\beta\beta;\alpha\rangle$ spin states ($F_z = -1/2$) increase. This is because the states $F_z = +1/2$ are populated due to ST_+RPM with less efficiency compared to the population of the $F_z = -1/2$ spin states due to ST_RP. The importance of the longitudinal spin relaxation is demonstrated by the observation that, at long times, the population of the $|\alpha\alpha;\alpha\rangle$ spin state is smaller than that of the $|\beta\beta;\beta\rangle$ (and even smaller than $|\beta\alpha;\beta\rangle$ and $|\alpha\beta;\beta\rangle$ spin states). The former is connected by spin relaxation with the faster depleting $|\alpha\beta;\alpha\rangle$ and $|\beta\alpha;\alpha\rangle$ states, while the latter is connected with the higher populated $|\alpha\beta;\beta\rangle$ and $|\beta\alpha;\beta\rangle$. At the very long times the relative populations do not depend on time because the rate of a spin-selective reaction is the slowest process in the system studied.

in the separate pairs. When the radical pair is in contact, the situation is dramatically different. Now the "inactive" $|\alpha\alpha;\beta\rangle$ and $|\beta\beta;\alpha\rangle$ states are mixed with the "active" $|\beta\alpha;\alpha\rangle$ and $|\alpha\beta;\beta\rangle$ states. This mixing is asymmetric since the rate of mixing in $F_z = +1/2$ and $F_z = -1/2$ manifolds is different, i.e., proportional to $A^2/4(\omega_0 - J_c)$ for the former and $A^2/4(\omega_0 + J_c)$ for the latter in the first order of perturbation theory ($\omega_0 \gg |J_c| \gg A$).

Thus, there are four key processes contributing to the observed polarization. First, the chemical decay of H atoms is the spin-selective reaction. The polarization cannot arise in random pairs if the chemical decay is nonspin-selective. Second, the ST_0RPM which is but the difference in populations between the $|\alpha\beta;\alpha\rangle$ and $|\beta\alpha;\alpha\rangle$ states for the low-field resonance (emission) and that of the $|\alpha\beta;\beta\rangle$ and $|\beta\alpha;\beta\rangle$ states (absorption) for the high-field one. Third, the depletion of the $|\alpha\alpha;\beta\rangle$ and $|\beta\beta;\alpha\rangle$ states causes positive polarization for the high-field resonance and negative polarization for the low-field resonance. Since the depletion of the former is faster than that of the latter, the emissive polarization can be much stronger at relatively short time, but it tends to equal intensities with long time. Taken together, the second and third points are the qualitative interpretation of the theory of the nonadiabatic spin transitions at magnetic fields, developed by Shushin.[23] Fourth is the longitudinal spin relaxation of the $|\alpha\alpha;\alpha\rangle$ and $|\beta\beta;\beta\rangle$ "inactive" states. If this relaxation could be neglected, the system with its strong hyperfine interaction and slow diffusion would inevitably arrive at the situation where the only populated states are the $|\alpha\alpha;\alpha\rangle$ and $|\beta\beta;\beta\rangle$. That would produce an EPR spectrum with equally intense negatively polarized low-field and positively polarized high-field resonance lines at long times (Figure 7).

Comparison of the longitudinal spin relaxation rates in the system with the overall rate of recombination $k_r = f_s Z\, k_s\tau_c/1 + k_s\tau_c$ (where f_s is the effective spin factor, close to 1/2 (not 1/4)[7] for the given system) shows that at all temperatures k_r falls far short of w_{1b}: $k_r/f_s = 1.8 \times 10^4 s^{-1}$, $w_{1b} + w_{1a} = 2.5 \times 10^5\ s^{-1}$ at low temperature, and $k_r/f_s = 1.2 \times 10^6 s^{-1}$, $w_{1b} = (4 - 8) \times 10^6\ s^{-1}$ at high temperature. The importance of this observation is not only in the conclusion that the kinetics of polarization is controlled by the chemical decay of pairs at the longest times. It is even more important that this relation between the rates of longitudinal spin relaxation and recombination of radicals prevents total depletion of the $|\alpha\beta;m_N\rangle$ and $|\beta\alpha;m_N\rangle$ states. The longitudinal spin relaxation not only reduces the intensity of polarization, but also populates (Figure 7) the "active" $|\beta\alpha,m_N\rangle$ and $|\alpha\beta,m_N\rangle$ states providing the conditions where the ST_0RPM can operate, i.e., result in the positive polarization of the high-field spectral line.

The importance of the relation between the $w_{1a} + w_{1b}$ and k_r is demonstrated by Figure 6B, where the thick solid line is the kinetics of positive polarization at low-temperature calculated with the parameters used to simulate experimental results. The thin solid line is calculated with the same parameters except that the $w_{1a} + w_{1b}$ are smaller by a factor of 4. When the rate of the longitudinal relaxation decreases, the positive polarization sharply increases at longer times due to the relative overpopulation of the inactive $|\beta\beta;\beta\rangle$ state in comparison with the $|\alpha\alpha;\beta\rangle$ state (Figure 7). This is the evidence for the importance of another source of positive polarization in addition to that provided by the ST_0RPM. The efficiency of this additional mechanism is defined by the efficiency of the $|\alpha\alpha;\beta\rangle$ state depopulation $Z \cdot A^2/8B_0^2$ (B_0R^2/D) $< w_{1a} + w_{1b}$caused by the sharing of the chemical activity with the $|\alpha\beta;\alpha\rangle$ state owing to the nonsecular part of the HFI (due to ST_+RPM polarization[23]). From a kinetic viewpoint this mechanism is distinguishable from the ST_0RPM. As a result the kinetic curves for the positive polarization demonstrate appearance of two poorly resolved extrema (Figures 2 and 6B). Since the negative polarization is dominated by the strong overpopulation of the $|\alpha\alpha;\alpha\rangle$ state in comparison with the $|\beta\alpha;\alpha\rangle$ state, these two extrema are not resolved in corresponding curves at all.

Figure 7 shows that the system arrives at the situation when the relative populations of states do not depend on time. This state (tail of the decay curve) is characterized by monoexponential decay with the rate constant k_r, while the relation between the positive and negative polarization does not depend on this parameter any longer. The time of observation of maximum negative polarization is controlled by the interplay between the rate of encounters Z, the rate of recombination k_r and the rate of longitudinal relaxation w_{1b}. It weakly depends on the intensity of exchange in the contact states while $|J_c| >$ A. The time of observation of maximum positive polarization coincides with that of negative polarization only for relatively fast longitudinal relaxation in radical pairs.

We found (Table 1) that the inequality $w_{1a} + w_{1b} < Z$ holds at any temperature. When the position of the extrema of polarization and the relation between their intensities were defined by the relation between J_c and $k_s\tau_c$ only, the kinetics could not be simulated without abandoning the restriction that $\tau_c Z$ does not depend on temperature.

Independence (or weak dependence) of the $k_s\tau_c$ on the temperature explains why the rate constant k_{dec} (see eq 1) exhibits an activation energy close to the activation energy of the H-atom diffusion. Indeed, since $k_s\tau_c \ll 1$, the overall rate constant for the H-atom chemical decay is equal to $k_r = f_s \times Z_0 \exp(-E_{diff}/RT) \times k_{s0} \exp(-E_s/RT)\tau_{c0} \exp(E_{diff}/RT) \approx (Z_0 \times k_{s0} \times t_{c0}) \exp(-E_s/RT) = (Z_0 k_{s0} t_{c0}) \exp(-E_{diff}/RT)$. The trend of experimental data to deviate from linearity in Arrhenius

parameters seen in Figure 3 now seems to be quite acceptable. This is because of the weak temperature dependence of the spin factor f_s and nonexact equivalence of the energies of activation of diffusion E_{diff} and that of reaction E_s. It is clear that more accurate experimental data are needed to make this discussion more productive.

6. Conclusion

Chemically induced dynamic electron-spin polarization (CIDEP) of H atoms in Vycor glass was investigated experimentally, and computationally modeled. It was found experimentally that the kinetics of the H atom's CIDEP and the relative intensities of the positive and negative polarizations in the water-saturated Vycor glass vary widely with the temperature.

The theoretical model to explain the experimental results is based on the idea that H atom's CIDEP is generated in radical pairs comprised of the H atom and a stable paramagnetic center. In that sense the model utilizes the theory of CIDEP developed for liquid solutions. The model is capable of quantitative simulation of experimental observations. It is shown that the longitudinal spin relaxation is of decisive importance for the manifestation of the ST_0RPM mechanism. It is also shown that the confined H atoms evolve to two totally coherent states $|\alpha;\alpha\rangle$ and $|\beta;\beta\rangle$ which provides another source of the positive polarization. Both of these processes are due to the inherent peculiarities of the confinement of the radical pairs.

The frequency of encounters, the rate constant of spin-selective recombination, and the intensity of exchange interaction, as well as the rates of longitudinal spin relaxation in pairs of the H-atom and its partner could be reasonably described using the model. At the same time it must be emphasized that all fits of experimental results in this paper were done with the approximation of zero spin-nonselective decay of pairs. The model predicts that the radical pairs are mostly random, i.e., the partner is created independently from the H atom.

Experimental observations of CIDEP in H atoms generated by electron irradiation of wet nanoporous materials are accounted for by the dynamic behavior of confined particles (molecules, radicals, etc.) within the nanometer scales. This is valuable information for the understanding of the chemical processes in such materials and for the issues concerned with the problems of spin communication in nanoconfined spin systems. The fact that the shape of kinetic curves strongly depends on the rates of the longitudinal spin relaxation allows for the corresponding measurements of the time scales, which are very inconvenient for standard experimental methods. The magnitude of exchange interaction between two paramagnetic particles available from the simulation represents unique method for obtaining such a valuable parameter of intermolecular interactions.

Among three possible mechanisms listed above for the effects of confinement on the CIDEP in H atoms, we have considered only one in this paper. We found that the restricted diffusion of H atoms within the confined water/ice accounts for the observed kinetics of CIDEP. Future research on the nanoporous materials will address the other possible scenarios and effects of nanoconfinement.

Acknowledgment. We thank Dr. D. M. Bartels for the discussion and proofreading of this manuscript.

References and Notes

(1) Chemerisov, C. D.; Trifunac, A. D. *Chem. Phys. Lett.* **2001**, *347*, 65.
(2) Chemerisov, S. D.; Werst, D. W.; Trifunac, A. D. *Rad. Phys. Chem.* **2001**, *60*, 405.
(3) Freed, J. H.; Pedersen, J. B. *Adv. Magn. Reson.* **1976**, *8*, 1.
(4) Adrian, F. J. *Rev. Chem. Intermed.* **1979**, *3*, 3.
(5) Bartels, D. M.; Han, P.; Percival, P. W. *Chem. Phys.* **1992**, *164*, 42; *Chem. Phys. Lett.* **1993**, *210*, 129.
(6) Bartels, D. M.; Chiu, T. M.; Trifunac, A. D.; Lawler, R. G. *Chem. Phys. Lett.* **1986**, *123*, 497.
(7) Shkrob, I. A.; Trifunac, A. D. *Phys. Rev.* B **1996**, *54*, 15073.
(8) Shkrob, I. A.; Tadjikov, B. M.; Chemerisov, S. D.; Trifunac, A. D. *J. Phys. Chem.* **1999**, *111*, 5124.
(9) Jorgensen, J. S.; Pedersen, J. B.; Shushin, A. I. *Chem Phys.* **1996**, *211*, 235.
(10) Tarasov, V. F.; Forbes, M. D. E. *Spectrochim. Acta* A **2000**, 56, 245.
(11) Trifunac, A. D.; Norris, J. R.; Lawler, R. G. *J. Chem. Phys.* **1979**, *71*, 4380.
(12) Griscom, D. L.; Stapelbroek, M.; Friebele, E. J. *J. Chem. Phys.* **1983**, *78*, 1638.
(13) Munekurini, S.; Yamanaka, T.; Shimogaichi, Y.; Nagasawa, K.; Hama, Y. *J. Appl. Phys.* **1990**, *68*, 1212.
(14) Schwarz, H. A. *J. Phys. Chem.* **1969**, *73*, 1928.
(15) Basmadjian D.; Chu, K. P. *Can. J. Chem.* **1964**, *42*, 946.
(16) Data on the average pore diameter were obtained from the Materials Business Corning Incorporated. Product Information. VYCOR Brand Porous Glass, 2000.
(17) Fouzri, A.; Dorbez-Sridi, R. Oumezzine, M. *J. Chem. Phys.* **2002**, *116*, 791.
(18) Waite, T. R. *Phys. Rev.* **1957**, *107*, 463.
(19) Adrian F. J.; Monchick, L. *J. Chem. Phys.* **1979**, *71*, 2600; *J. Chem. Phys.* **1980**, *72* , 5786. Alexandrov, I. V. *Zh. Eksp. Teor. Fiz.* **1971**, *60*, 1273 (Russian).
(20) Shushin, A. I. *Chem. Phys.* **1990**, *144*, 201, 223.
(21) Golub, G. H.; van Loan, C. F. *Matrix Computations*, The Johns Hopkins University Press: Baltimore, 1996.
(22) Bagryanskaya, E. G.; Sagdeev, R. Z. *Russ. Chem. Rev.* **2000**, *69*, 925.
(23) Shushin, A. I. *Chem. Phys. Lett.* **1995**, *237*, 177.
(24) Tarasov, V. F.; Yashiro, H.; Maeda, K.; Azumi, T.; Shkrob I. A. *Chem. Phys.* **1998**, *226*, 253.